



Formation of Al containing molecular complexes in the gas phase in dense molecular clouds: quantum study of the radiative association of $\text{Al}^+ + \text{H}_2$ and $\text{Al}^+ + \text{D}_2$

Daria Jones (nee Burdakova),¹ Gunnar Nyman¹ and Thierry Stoecklin^{2*}

¹Department of Chemistry and Molecular Biology, University of Gothenburg, SE-41296 Gothenburg, Sweden

²Université de Bordeaux, ISM, UMR 5255, F-33405 Talence, France

Accepted 2021 March 2. Received 2021 February 25; in original form 2021 January 13

ABSTRACT

Radiative association (RA) of Al^+ with H_2 is the first step in the formation of AlH in gas phase and is here investigated theoretically. We use recent potential energy and dipole moment surfaces and a quantum approach based on the driven equations formalism for performing the dynamics for both the $\text{Al}^+ - \text{H}_2$ and $\text{Al}^+ - \text{D}_2$ systems. The obtained RA rate coefficients are compared with previous evaluations based on transition state theory and found to be orders of magnitude larger. They are also compared to those obtained recently for the similar systems $\text{Na}^+ - \text{H}_2/\text{D}_2$. The possible role played by RA of Al^+ with H_2 in the gas phase chemistry of dense molecular clouds is discussed.

Key words: astrochemistry – molecular data – molecular processes – scattering – ISM: molecules.

1 INTRODUCTION

Gas phase reactions involving metals is a relatively new topic in astrochemistry as metals were believed to accumulate on dust grains and seldom participate in gas phase reactions. When several gas phase molecules containing metals (NaCl , AlCl , KCl , AlNC , AlO , AlOH , AlF , Na(CN) , MgCN , MgNC) were observed in the envelope of IRC+10216 (Cernicharo & Guelin 1987; Kawaguchi et al. 1993; Turner, Steimle & Meerts 1994; Ziurys, Apponi & Phillips 1994; Ziurys et al. 1995; Tenenbaum et al. 2010), it proved that metals can form molecules in the interstellar medium. AlO has also been found in stellar photospheres, both in absorption and emission via its electronic transitions (Kamínski et al. 2016).

AlH is one of the simplest hydrogen-metal systems that is yet to be detected. Considering the relatively high abundance of aluminum (3×10^{-6}) together with the fact that aluminum bonded to a rarer element such as fluorine or chlorine has been detected, the AlH molecule may be expected to be present as well.

As discussed in a previous paper (Burdakova, Nyman & Stoecklin 2019) dedicated to the formation of NaH , the gas phase mechanism mentioned already by Kirby & Dalgarno (1978) consists of two steps. The first step, here written for a general atomic metal ion M^+ , is the radiative association of it with H_2 :



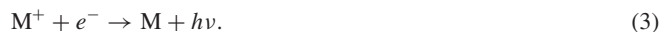
followed by a dissociative recombination step with an electron:



In this study, formation of AlH through this route is investigated.

Association reactions containing metal ions can have a big impact on interstellar chemistry even if they do not produce a significant amount of molecules containing metals. This is due to the fact that most models of cloud chemical evolution assume very low abundances of metal ions since if higher abundances of metals ions were assumed this would also mean that the abundance of free electrons would be higher, which, in turn, would limit the chemical evolution of H, C, N, O, and S via ion/molecule reactions ((Mitchell 1978; Graedel, Langer & Frerking 1982).

The recombination coefficients of atomic metal ions with an electron are typically $\sim 10^{-12} \text{ cm}^3 \text{ s}^{-1}$, while for molecular metal ions, they are $\sim 10^{-6} \text{ cm}^3 \text{ s}^{-1}$ (Ip & Axford 1986). In other words, the dissociative recombination described by equation (2) is much faster than radiative recombination (RR) of a metal ion in atomic form with an electron:



This means that having the metal ions in molecular rather than atomic form would lead to faster neutralization. This would, in turn, allow the model to include a higher abundance of metals (Petrie & Dunbar (2000)).

Knowing the fractional abundance f_e of electrons relative to H_2 and the RR rate coefficient $k_{\text{RR}}^{e^-}$ with electrons and following arguments of Smith et al. (1983) a minimum value of the RA rate coefficient k_{RA} with H_2 for which the RA process could compete with the RR process can be deduced:

$$k_{\text{RA}}^{\text{H}_2} \geq k_{\text{RR}}^{e^-} \times f_e. \quad (4)$$

The RA rate constant for the formation of $\text{Al}^+ - \text{H}_2$ has been previously calculated by Petrie & Dunbar (2000) using the transition state theory. For the temperatures 10, 30, and 100 K, they obtained the reaction rate constants 1.3×10^{-23} , 8.6×10^{-24} , and $4.5 \times 10^{-24} \text{ cm}^3 \text{ molecule}^{-1} \text{ s}^{-1}$, respectively. These relatively small values

* E-mail: thierry.stoecklin@u-bordeaux.fr

would exclude the formation of AIH through radiative association in molecular clouds.

Our previous study dedicated to the formation of Na^+-H_2 and Na^+-D_2 through RA showed that the transition state estimate of the RA rate coefficient was several orders of magnitude smaller than the value obtained using close coupling (CC) calculations. The CC reaction rate constant was also significantly closer to the experimental value. It is therefore the purpose of this paper to check if CC calculations may provide large enough RA rates for the Al^+-H_2 and Al^+-D_2 systems to support the hypothesis of production of AIH and AID in the gas phase through radiative association in molecular clouds.

Recent investigations of the Al^+-H_2 and Al^+-D_2 complexes were performed by Emmeluth et al. (2007). They performed experimental measurements and *ab initio* calculations of the rotationally resolved ro-vibrational spectrum of these two complexes. Very good agreement between theory and experiment was obtained, which demonstrated the high accuracy of their potential energy surface (PES). In this work, we use their 3D PES and dipole moment surfaces to study the radiative association of these two complexes.

Numerous CC radiative association calculations have been performed on the formation of diatoms (HD , HF , OH , NH , CH^+ , CF^+ , CN , CO , O_2 , AlCl , NaCl , etc.); see, for example, Szabo & Gustafsson (2019), Andreazza, Almeida & Vichiatti (2018), Öström et al. (2016), and Stancil & Dalgarno (1997) and the review by Nyman, Gustafsson & Antipov (2015) and reference therein. In contrast, available calculations for triatomic systems are limited to the six systems: H_2^+-He (Mrugala, Spirko & Kraemer 2003), H^--H_2 (Ayoub et al. 2011), H^--N_2 (Stoecklin, Lique & Hochlaf 2013), $\text{H}-\text{CO}$ (Stoecklin et al. 2018b), H^--CO (Stoecklin et al. 2018a), and H_2-Na^+ (Burdakova et al. 2019). The method developed in (Stoecklin et al. 2013) was used in the last three of the above-mentioned works and is also applied in this study.

This paper is organized as follows: In Section 2, we briefly describe the main features of both the PES and the dipole moment surface calculated by Emmeluth et al. (2007) and we summarize the main steps of the method used to calculate the RA rate coefficients. In Section 3, we present and discuss our results and their implication for the importance of the RA processes forming Al^+-H_2 and Al^+-D_2 in the chemistry of molecular clouds. Conclusions are found in Section 4.

2 METHODS

As in our previous paper (Burdakova et al. 2019), our calculations are performed using reactant Jacobi coordinates (R, r, θ) where R is the intermolecular distance, r the bond length of the diatom, and θ the angle between r and R .

2.1 Potential energy surface and dipole moment

We use the *ab initio* potential energy surface (PES) and dipole moment surface (DMS) developed for this system by Emmeluth et al. (2007). They are based on a grid of 400 points computed at the coupled cluster CCSD(T) level of theory and using the aug-cc-pVQZ basis set and a set of 3s3p2d2f1g bond functions located at the midpoint of the intermolecular axis. The *ab initio* grid includes six r grid points ranging from 1.0 to 2.2 bohr, 40 values of R in the 2.75–40.0 bohr interval, and the four bond angles 0° , 30° , 60° , and 90° . Emmeluth et al. (2007) obtained an analytical model of the PES, depicted in Fig. 1, by fitting the *ab initio* grid, which describes accurately the short and long range expected asymptotic behaviours as well as the region of the well. The equilibrium geometry of the

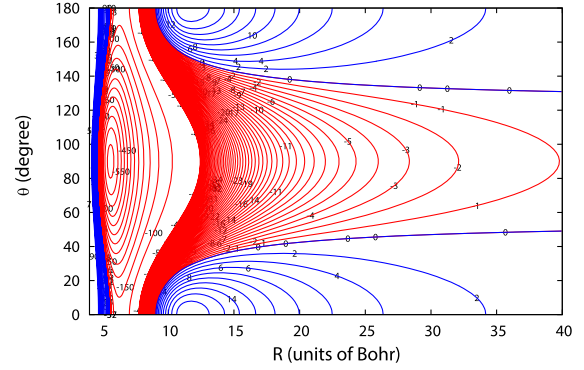


Figure 1. Contour plots of the potential energy surface of Al^+-H_2 obtained by Emmeluth et al. for $r = 1.4097a_0$. The energy is given in cm^{-1} .

Al^+H_2 complex is found to be T shaped by the authors (Emmeluth et al. 2007) with $R = 5.726$ bohr and an H_2 bond distance of 1.4097 bohr, which is only 0.009 bohr larger than the bond length of a free H_2 molecule. This latter result suggest that the use of the rigid rotor approximation could be appropriate for this system.

The minimum potential energy is 668.4 cm^{-1} below the reactants, while the binding energies of the Al^+-H_2 complex are 469.4 and 506.4 cm^{-1} for the para- and ortho-species, respectively.

2.2 Bound states and dynamics

We use the method initially presented in Stoecklin et al. (2013) and there applied to formation of N_2H^- by RA. More details can be found in that paper. It is based on the driven equation formalism that connects the bound and scattering wave functions through the light-matter interaction operator.

The initial $\Psi_i^{JM}(R, r, \theta)$ and final $\Psi_f^{\alpha J'M'}(R, r, \theta)$ space fixed wave functions are written in the same set of Jacobi coordinates:

$$\Psi_i^{JM}(R, r, \theta) = \frac{1}{Rr} \sum_{v,j,l} \chi_{v,j,l}^{JM}(R) \varphi_{vj}(r) Y_{jl}^{JM}(\hat{R}, \hat{r}), \quad (5)$$

$$\Psi_f^{\alpha J'M'}(R, r, \theta) = \frac{1}{Rr} \sum_{v',j',l'} \omega_{v',j',l'}^{\alpha J'M'}(R) \varphi_{v'j'}(r) Y_{j'l'}^{J'M'}(\hat{R}, \hat{r}), \quad (6)$$

where j , l , and J are, respectively, the quantum numbers associated with the rotational, orbital and total angular momenta of the system, while α denotes a given bound state. $\chi_{v,j,l}^{JM}(R)$ and $\omega_{v',j',l'}^{\alpha J'M'}(R)$ are the R -dependent radial parts of the initial and final wave functions while $\varphi_{vj}(r)$ represents the r dependent ro-vibrational parts.

The wave functions are expanded in the same coupled angular basis sets:

$$Y_{jl}^{JM}(\hat{r}, \hat{R}) = \sum_{m_j, m_l} \langle jm_j lm_l || JM \rangle y_j^{m_j}(\hat{r}) y_l^{m_l}(\hat{R}). \quad (7)$$

2.2.1 Bound state calculations

The bound states are calculated using 400 Chebyshev DVR grid points in the range $[3-80]a_0$ for describing the radial part R of the wavefunction. Eighteen Gauss–Hermite points in the range $[0.725-2.09]a_0$ are used for the vibrational coordinate r , along with 10 rotational basis functions (Legendre polynomials) for each nuclear spin isomer of H_2 and D_2 . Thus, j ranges from 0 to 18 for para- H_2 and ortho- D_2 , and from 1 to 19 for ortho- H_2 and para- D_2 .

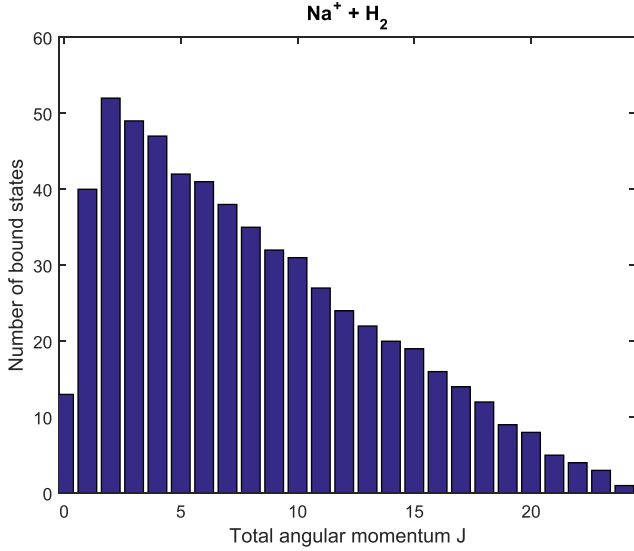


Figure 2. Number of bound states of Al^+-H_2 as a function of the total angular momentum quantum number of the system.

2.2.2 Dynamics

The radial part of the total wavefunction describing the system before and after radiative association is a solution of the following equation:

$$\left[\frac{d^2}{dR^2} - \frac{l(l+1)}{R^2} + k_{vj}^2(E) - U_{vj}^{v'j'l'}(R) \right] \chi_{vj}^{v'j'l'}(R) = \lambda_{vj}^{\alpha J' M'}(R), \quad (8)$$

where $U_{vj}^{v'j'l'}(R)$ are the matrix elements of the intermolecular potential, k_{vj} are channel wave vectors, and the right-hand side of equation (8), $\lambda_{vj}^{\alpha J' M'}(R)$, represents the driving terms, which are real and result from the dipolar couplings of the initial and scattering wave functions. Within the dipolar approximation,

$$\lambda_{vj}^{\alpha J' M'}(R) = -2\mu_{\text{Al}^+-\text{H}_2} \int d\hat{r} d\hat{r}' \varphi_{vj}(r) Y_{jl}^{JM}(\hat{r}, \hat{R}) \times \mu(\vec{R}, \vec{r}) \Psi_f^{\alpha, J', M'}(R, r, \theta). \quad (9)$$

For a charged atom interacting with a neutral homonuclear diatom, the dipole moment of the system can safely be assumed to lie along the intermolecular axis R . This approximation was previously found to give results in very good agreement with the *ab initio* dipole moments calculated for the H^--N_2 (Stoecklin et al. 2013) and Na^+-H_2 (Burdakova et al. 2019) complexes. It is found to also perform well for Al^+-H_2 when compared with the *ab initio* dipole calculated by Emmeluth et al. (2007). The scattering wavefunction is propagated using the Magnus propagator from the classically forbidden region out to the asymptotic region where an incoming plane wave boundary condition is applied. The radiative association cross-section for a given initial ro-vibrational state (v, j) of H_2 is then obtained from the following expression (corrected of a typo in Burdakova et al. 2019):

$$\sigma_{v,j}(E) = \frac{8\pi^2}{3k_{vj}^2 c^3} \sum_{J, J', \alpha} \omega_\alpha^3 \left[M_{v,j,J}^{\alpha, J'}(E) \right]^2, \quad (10)$$

where ω_α is the angular frequency of the emitted photon and $M_{v,j,J}^{\alpha, J'}(E)$ are obtained by integrating state-selected driving terms $\lambda_{vj}^{\alpha J' M'}(R)$ over R and summing over the indices M , l and M' .

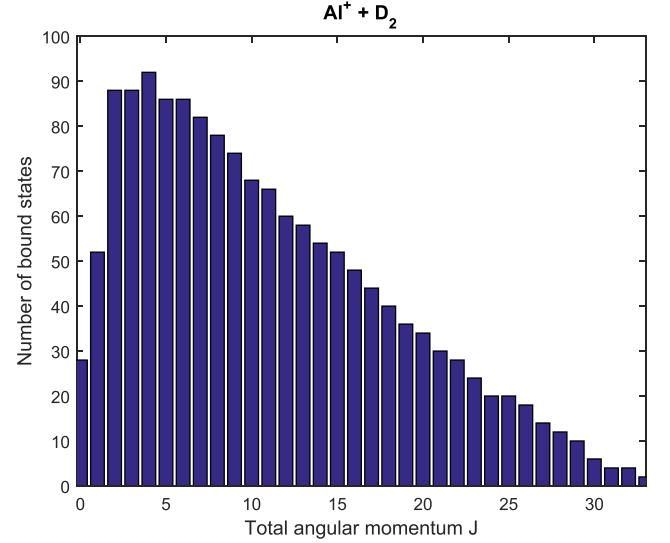


Figure 3. Number of bound states of Al^+-D_2 as a function of the total angular momentum quantum number of the system.

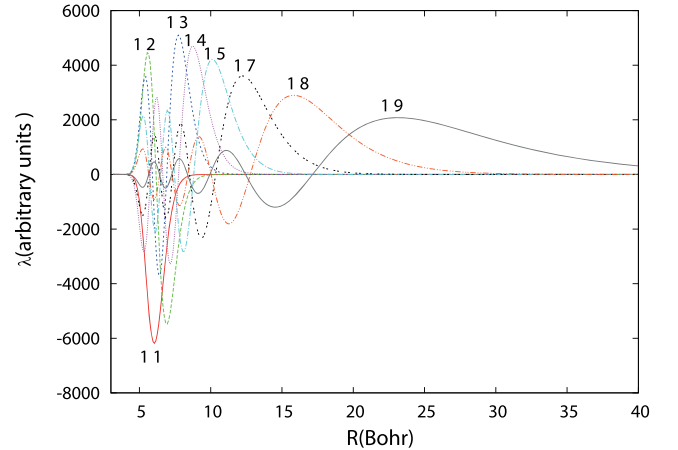


Figure 4. Variation of the $l = 0$ component of the $J = 0$ driving terms ($\lambda_{v=0, j=0, l=0, J=0}^{\alpha, J'=1}(R)$) as a function of the intermolecular coordinate for a collision energy of 1 cm^{-1} . The two numbers reported on each curve are the quantum numbers J' and α of the final bound state.

3 RESULTS

Similarly to previous studies the para- and ortho-spin isomers of H_2 and D_2 were treated separately. States lying above the zero-point energy level of the reactants but with no open rotational predissociation channels are treated as bound states. This results in 311 para- and 293 ortho-bound states needing to be included in the Al^+-H_2 RA calculations. For Al^+-D_2 RA calculations, these numbers are more than doubled with 753 para- and 721 ortho-bound states.

Figs 2 and 3 show, respectively, the variation of the calculated number of bound states of Al^+-H_2 and Al^+-D_2 as a function of the total angular momentum quantum number J . The total number of bound states is 604 for Al^+-H_2 and 1474 for Al^+-D_2 , while the largest value of J resulting in a bound state is 24 for the Al^+-H_2 and 33 for Al^+-D_2 .

Figs 4 and 5 illustrate the variation of the driving term $\lambda_{v=0, j=0, l=0, J=0}^{\alpha, J'=1}(R)$ as a function of the intermolecular distance, respectively for $(J =$

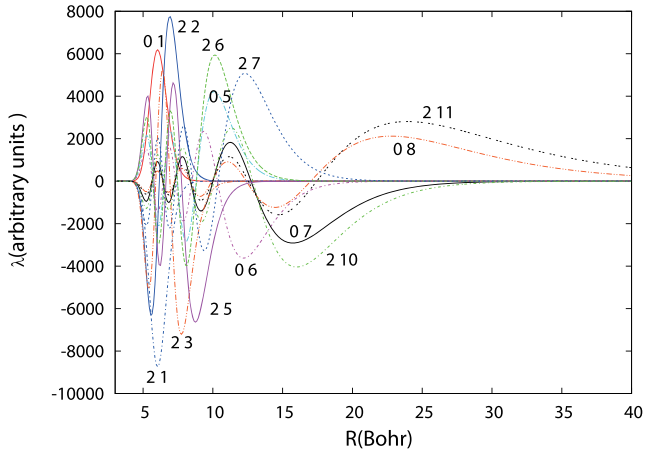


Figure 5. Variation of the $l = 2$ component of the ($J = 1$, $\varepsilon = -$) driving terms ($\lambda_{v=0, j=2, l=2, J=1}^{\alpha, J'}(R)$) as a function of the intermolecular coordinate for a collision energy of 1 cm^{-1} . The two numbers reported on each curve are the quantum numbers J' and α of the final bound state.

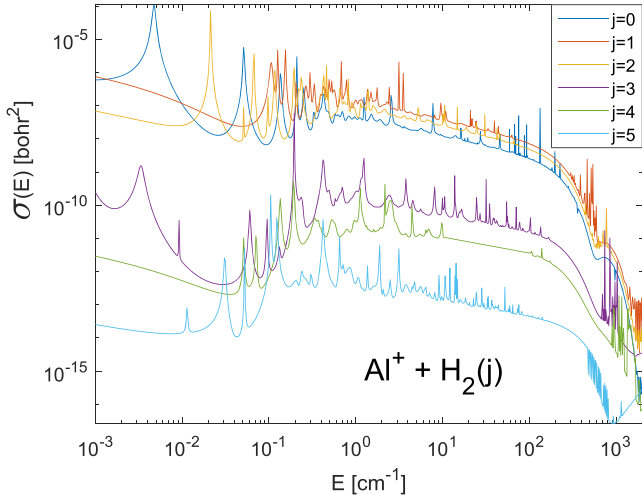


Figure 6. Radiative association cross-section of $\text{Al}^+ - \text{H}_2$ as a function of collision energy depicted for different values of j .

0 , $\varepsilon = +$) and ($J = 1$, $\varepsilon = -$) at a collision energy of 1 cm^{-1} . Clearly, the lower bound states that are localized in a narrower intermolecular distance interval give a localized driving term, while the most excited bound states extend over a large intermolecular range and give rise to an extended domain of the driving term. The present $\text{Al}^+ - \text{D}_2$ driving terms are also seen to be localized in a narrower intermolecular distance interval than those of the $\text{Na}^+ - \text{H}_2$ system (Burdakova et al. 2019). As the cross-section is directly proportional to the square of the integral of the contributing driving terms (λ) at a given collision energy, this will have impact on the cross-sections.

The variation as a function of collision energy of the $\text{Al}^+ - \text{H}_2$ and $\text{Al}^+ - \text{D}_2$ RA cross-sections is presented in Figs 6 and 7 for various initial rotational states of the diatomic fragments. These figures are very similar to those obtained previously for the $\text{Na}^+ - \text{H}_2$ and $\text{Na}^+ - \text{D}_2$ systems (Burdakova et al. 2019), while the magnitude of the cross-sections involving Al^+ are smaller. This can be understood by comparing the PES and the bound states of these systems. The $\text{Na}^+ - \text{H}_2$ PES is deeper than the one of $\text{Al}^+ - \text{H}_2$. As a result, the number of bound states of $\text{Al}^+ - \text{H}_2$ is smaller. The lowest bound state energies are

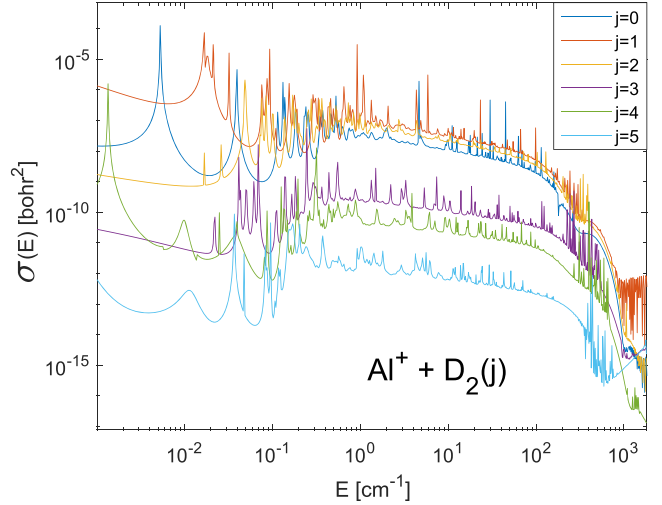


Figure 7. Radiative association cross-section of $\text{Al}^+ - \text{D}_2$ as a function of collision energy depicted for different values of j .

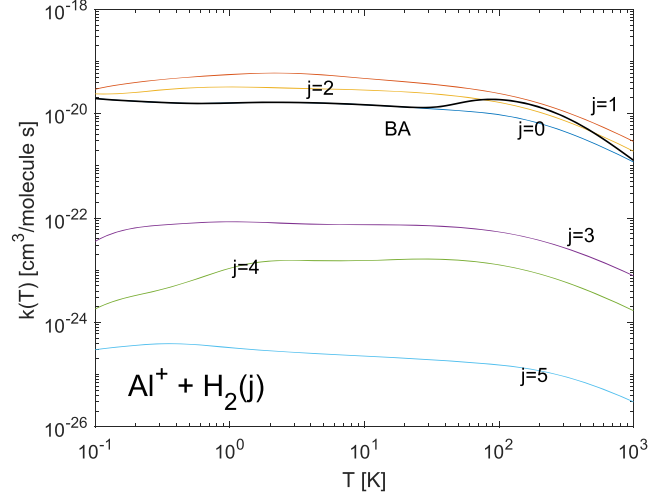


Figure 8. Radiative association rate coefficient for forming $\text{Al}^+ - \text{H}_2$ as a function of temperature depicted for different values of j .

also quite different (-844.37 cm^{-1}) for $\text{Na}^+ - \text{H}_2$ and (-461.81 cm^{-1}) for $\text{Al}^+ - \text{H}_2$. We note that the cross-section is proportional to ω^3 .

The mentioned features reduce the $\text{Al}^+ - \text{H}_2/\text{D}_2$ RA cross-sections compared to those of $\text{Na}^+ - \text{H}_2/\text{D}_2$ by about two orders of magnitude. We also notice that the initial rotational state $j = 1$ gives the largest $\text{Al}^+ - \text{H}_2/\text{D}_2$ RA cross-sections, while it is the initial rotational state $j = 2$ for the $\text{Na}^+ - \text{H}_2/\text{D}_2$ RA cross-sections.

j -resolved RA rate coefficients are presented in Figs 8 ($\text{Al}^+ - \text{H}_2$) and 9 ($\text{Al}^+ - \text{D}_2$). In both figures, the total Boltzmann-averaged reaction rate constants are also reported. A ratio of 2:1, obtained from the spin statistics was included when combining the ortho- D_2 and para- D_2 rate coefficients, while a ratio of 3:1 was used when combining the ortho- H_2 and para- H_2 rate coefficients.

For both reactions, the Boltzmann-averaged rate coefficients are seen to be almost flat at low temperature before reaching a maximum close to 87 K for $\text{Al}^+ - \text{H}_2$ formation while two less marked maxima are visible at 5 and 43 K for the $\text{Al}^+ - \text{D}_2$ formation. Both rate coefficients thereafter decrease monotonously and follow the expected T^{-1} law predicted by the modified thermal theory. This general behaviour

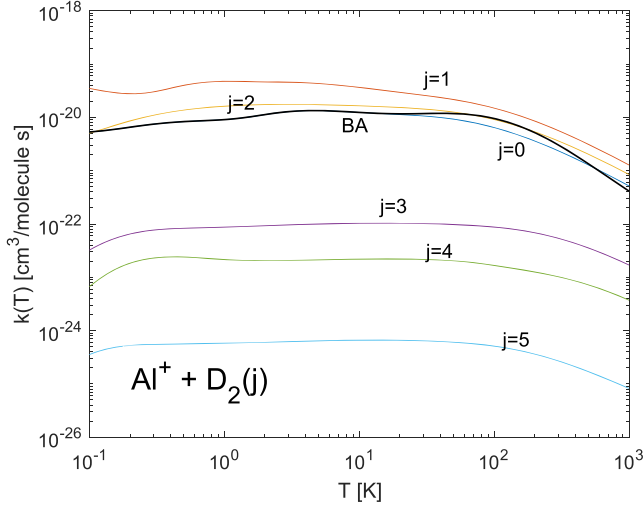


Figure 9. Radiative association rate coefficient for forming $\text{Al}^+\text{-D}_2$ as a function of temperature depicted for different values of j .

Table 1. Comparison between the CC RA rate coefficients obtained in this study with the ones calculated by Petrie and Dunbar using the transition state theory.

Temperature (K)	$r(T)$ (Petrie et al.)	$r(T)$ (this study)
10	1.3×10^{-23}	1.5×10^{-20}
30	8.6×10^{-24}	1.3×10^{-20}
100	4.5×10^{-24}	1.9×10^{-20}

Note. The rate coefficients are given in $\text{cm}^3 \text{ molecule}^{-1} \text{ s}^{-1}$.

was also obtained and analysed for similar ionic complexes like $\text{N}_2\text{-H}^-$ (Stoecklin et al. 2013) and $\text{Na}^+\text{-H}_2$ (Burdakova et al. 2019).

Above 10 K, the largest $\text{Al}^+\text{-H}_2$ RA rate constant is $1.9 \times 10^{-20} \text{ cm}^3 \text{ molecule}^{-1} \text{ s}^{-1}$ at $T = 87$, while it is $1.2 \times 10^{-20} \text{ cm}^3 \text{ molecule}^{-1} \text{ s}^{-1}$ at 43 K in the case of the $\text{Al}^+\text{-D}_2$ RA. For forming the $\text{Na}^+\text{-H}_2$ and $\text{Na}^+\text{-D}_2$ complexes, we obtained maximum values of about $5 \times 10^{-18} \text{ cm}^3 \text{ molecule}^{-1} \text{ s}^{-1}$ at $T = 200$ K and $7 \times 10^{-20} \text{ cm}^3 \text{ molecule}^{-1} \text{ s}^{-1}$ at 100 K. There is thus a big difference in the isotope effect for the $\text{Al}^+\text{-D}_2/\text{Al}^+\text{-H}_2$ systems and the $\text{Na}^+\text{-D}_2/\text{Na}^+\text{-H}_2$ systems. The $\text{Na}^+\text{-D}_2/\text{Na}^+\text{-H}_2$ systems show a strong isotope effect, while the maximum RA rate coefficient for forming the $\text{Al}^+\text{-D}_2$ complex is much closer to the one for forming the $\text{Al}^+\text{-H}_2$ complex.

The reaction rate constants for formation of the $\text{Al}^+\text{-H}_2$ molecule have been previously calculated by Petrie & Dunbar (2000) based on transition state theory. A comparison between their results and ours is presented in Table 1. At 10 K, our CC rate coefficient is seen to be three orders of magnitude larger than the one of Petrie & Dunbar (2000), while at 100 K, our value is almost four orders of magnitude larger than theirs. This difference is however not large enough to question their conclusion that RA forming $\text{Al}^+\text{-H}_2$ is too slow to matter in astrochemistry.

We can indeed evaluate the maximum fractional abundance of electrons f_e^{max} , which makes RA important for the chemistry of an interstellar cloud, using equation (4). For this purpose, we need to know the RR rate of Al^+ with an electron, which unfortunately is not available. However, as RR rates depend only weakly on the nature of the positive ion (Biondi 1969), we can use the expression given by Prasad & Huntress (1980) for Na^+ , $k_{\text{RR}}^e(T) = 2.7 \times 10^{-12}(T/300)^{-0.69} \text{ cm}^3 \text{ s}^{-1}$. The maximum fractional abun-

Table 2. Maximum electron fractional abundance f_e^{max} relative to H_2 for which the radiative association to form $\text{Al}^+\text{-H}_2$ would be more efficient than radiative recombination of Al^+ with an electron for two temperatures.

T (K)	k_{RA}	k_{RR}	f_e^{max}
10	1.5×10^{-20}	2.8×10^{-11}	5.4×10^{-10}
100	1.9×10^{-20}	5.8×10^{-12}	3.3×10^{-9}

Note. The RA and RR rate coefficients are given in $\text{cm}^3 \text{ molecule}^{-1} \text{ s}^{-1}$.

dance of electrons f_e^{max} for which the RA rate for forming $\text{Al}^+\text{-H}_2$ would be more efficient than RR of Al^+ with an electron f_e^{max} is reported in Table 2 for 10 and 100 K. These values of f_e^{max} appear to be an order of magnitude smaller than the usual estimate of the fractional abundance of electrons relative to H_2 in dense molecular clouds.

We conclude, following the arguments used by Smith et al. (1983) leading to equation (4), that the $\text{Al}^+\text{-H}_2$ RA rate coefficients are not large enough for this mode of production of AlH in the gas phase to need to be included in the chemistry models of dense molecular clouds.

4 CONCLUSION

The formation of $\text{Al}^+\text{-H}_2$ and $\text{Al}^+\text{-D}_2$ through RA was investigated theoretically at the close-coupling level using a recent 3D PES and dipole moment surface. The total number of bound states obtained for the $\text{Al}^+\text{-D}_2$ molecule is more than twice as large as for the $\text{Al}^+\text{-H}_2$ molecule. This is due to the mass difference between the two systems. This also affects the largest value of J resulting in a bound state. For the $\text{Al}^+\text{-H}_2$ molecule, the largest value of J is 24 while it is 33 for the $\text{Al}^+\text{-D}_2$ molecule.

The $\text{Na}^+\text{-H}/\text{-D}_2$ system that we recently investigated (Burdakova et al. 2019) was found to exhibit a very strong isotope effect, while the RA rate constants of $\text{Al}^+\text{-D}_2$ and $\text{Al}^+\text{-H}_2$ are of the same magnitudes. The $\text{Al}^+\text{-H}_2/\text{D}_2$ RA rate coefficient are furthermore found to be two orders of magnitude smaller than those of $\text{Na}^+\text{-H}_2/\text{D}_2$ as a result of a globally less attractive potential.

Our rate coefficient for forming $\text{Al}^+\text{-H}_2$ at 100 K is almost four orders of magnitude larger than the available transition state estimate of Petrie & Dunbar (2000). However, following the arguments used by Smith et al. (1983), we confirm that the $\text{Al}^+\text{-H}_2$ RA rate coefficients are not large enough for this mode of production of AlH in the gas phase to need to be included in chemistry models of dense molecular clouds.

ACKNOWLEDGEMENTS

We gratefully acknowledge support from the Swedish Research Council (grant number 2016-03275). The calculations were performed at the Mesocentre de Calcul Intensif Aquitaine computing facilities of the Université de Pau et des Pays de l'Adour.

5 DATA AVAILABILITY

The data underlying this study are available in this paper.

REFERENCES

- Andreazza C. M., Almeida A. A., Vichiatti R. M., 2018, *MNRAS*, 477, 548
 Ayouz M., Lopes R., Raoult M., Dulieu O., Kokouline V., 2011, *Phys. Rev. A*, 83, 052712

- Biondi M. A., 1969, *Can. J. Chem.*, 43, 1711
- Burdakova D., Nyman G., Stoecklin T., 2019, *MNRAS*, 485, 5874
- Cernicharo J., Guelin M., 1987, *A&A*, 183, L10
- Emmeluth C., Poad B. L. J., Thompson C. D., Weddle G., Bieske E. J., Buchachenko A. A., Grinev T. A., Klos J., 2007, *J. Chem. Phys.*, 127, 164310
- Graedel T. E., Langer W. D., Frerking M. A., 1982, *ApJS*, 48, 321
- Ip W. H., Axford W. I., 1986, *Nature*, 321, 682
- Kamínski T. et al., 2016, *A&A*, 592, A42
- Kawaguchi K., Kagi E., Hirano T., Takano S., Saito S., 1993, *ApJ*, 406, L39
- Kirby K., Dalgarno A., 1978, *ApJ*, 224, 444
- Mitchell G. F., 1978, *AJ*, 83, 1612
- Mrugala F., Spirko V., Kraemer W. P., 2003, *J. Chem. Phys.*, 118, 10547
- Nyman G., Gustafsson M., Antipov S. V., 2015, *Int. Rev. Phys. Chem.*, 34, 385
- Öström J., Bezrukov D. S., Nyman G., Gustafsson M., 2016, *J. Chem. Phys.*, 144, 249901
- Petrie S., Dunbar R. C., 2000, *J. Phys. Chem. A*, 104, 4480
- Prasad S. S., Huntress J. W. T., 1980, *ApJS*, 43, 1
- Smith D., Adams G., Alge E., Herbst E., 1983, *ApJ*, 272, 365
- Stancil P. C., Dalgarno A., 1997, *ApJ*, 490, 76
- Stoecklin T., Halvick P., Lara-Moreno M. d. J., Trabelsi T., Hochlaf M., 2018a, *Faraday Discuss*, 212, 101
- Stoecklin T., Halvick P., Yu H.-G., Nyman G., Ellinger Y., 2018b, *MNRAS*, 475, 2545
- Stoecklin T., Lique F., Hochlaf M., 2013, *Phys. Chem. Chem. Phys.*, 15, 13818
- Szabo P., Gustafsson M., 2019, *MNRAS*, 483, 3574
- Tenenbaum E. D., Dodd J. L., Milam S. N., Woolf N. J., Ziurys L. M., 2010, *ApJS*, 190, 348
- Turner B. E., Steimle T. C., Meerts L., 1994, *ApJ*, 426, L97
- Ziurys L. M., Apponi A. J., Guélin M., Cernicharo J., 1995, *J. Astrophys.*, 445, L47
- Ziurys L. M., Apponi A. J., Phillips T. G., 1994, *ApJ*, 433, 729

This paper has been typeset from a \LaTeX file prepared by the author.